

THE ELLIPTICITY DISTRIBUTION OF AMBIGUOUSLY BLENDED OBJECTS

WILLIAM A. DAWSON¹, MICHAEL D. SCHNEIDER^{1,2}, J. ANTHONY TYSON², M. JAMES JEE²

(Dated: Draft December 3, 2024)
LLNL-JRNL-654061-Draft

ABSTRACT

Using overlapping fields with space-based Hubble Space Telescope (HST) and ground-based Subaru Telescope imaging we identify a population of blended galaxies that would not be easily distinguished with ground-based monochromatic imaging alone, which we label as ‘ambiguous blends’. For the depth targeted with the Large Synoptic Survey Telescope (LSST), the ambiguous blend population is both large ($\sim 14\%$) and has a distribution of ellipticities that is markedly different from that of unblended objects in a way that will likely be important for the weak lensing measurements. Most notably, we find that ambiguous blending results in a $\sim 14\%$ increase in shear noise (or $\sim 12\%$ decrease in n_{eff}) due to 1) larger intrinsic ellipticity dispersion, 2) a scaling with the galaxy number density N_{gal} that is shallower than $1/\sqrt{N_{\text{gal}}}$. For the LSST Gold Sample ($i < 25.3$) there is a $\sim 7\%$ increase in shear noise (or $\sim 7\%$ decrease in n_{eff})

Subject headings: cosmology: miscellaneous — galaxies: general — gravitational lensing: weak

1. INTRODUCTION

Weak gravitational lensing is entering the realm of precision cosmology where measurement accuracy becomes as important as measurement precision. Future surveys, such as the LSST³, will image billions of galaxies that can be used in gravitational lensing measurements. Most estimators of the gravitational lensing shear of a galaxy image are known to be systematically biased due to non-symmetric noise distributions (“noise bias”) (Kacprzak et al. 2012), imperfect knowledge of the unlensed galaxy shapes (“model-fitting bias”) (Voigt & Bridle 2010; Bernstein 2010), among other effects not well-understood.

The noise bias can be avoided by probabilistic algorithms (Bernstein & Armstrong 2014) that avoid the use of biased shear estimators, but at the expense of requiring prior knowledge of the distribution of unlensed intrinsic galaxy shapes. Much of our current characterization of the intrinsic ellipticity distribution of galaxies comes from space based observatories that have significantly different systematics from ground based observatories.

One such systematic is object blending, which affects ground-based observations more than space-based observations due to the $\sim 0.7''$ atmospheric seeing vs. $\sim 0.1''$ PSF from space. In addition to the PSF dependence, blending is also a function of: centroid separation, surface brightness profile, and object number density. It is important to make the distinction between different definitions of number density. From a theoretical standpoint it is most convenient to consider the raw number density defined at the limiting surface brightness of the survey, n . This is similar to what might be observed from a space-based survey, and can be several times larger than the number density observed from the ground. While blend-

ing will affect various subsamples differently, it makes most sense to work with n rather than the number density of a particular subsample since objects within the subsample will likely be blended with objects outside the subsample.

The degree to which objects are blended is a continuum, however we find it valuable to define three discrete classes of blends. We define *ambiguous blends* as two or more blended objects that overlap to such a degree that they are detected as a single object, *conspicuous blends* as two or more blended objects that overlap significantly but are detected as individual objects, and *innocuous blends* as two or more objects that may overlap in the outer periphery of their isophotes but to such a small degree that the overlap has no significant effect on the inferred properties of the objects. This paper will focus on the properties of ambiguous blends and consider all other objects ‘non-blends’.

In optical astronomy most existing work has been concerned with the detection and treatment of conspicuous blends (e.g. Beard et al. 1990; Bertin & Arnouts 1996, and references therein). For weak lensing, existing studies have been limited to considering how the surface number density of galaxies is decreased after removing conspicuous blends from the sample and the resulting impact on the lensing signal-to-noise (e.g. Miller et al. 2013; Chang et al. 2013). In other fields of astronomy (e.g. infrared, sub-mm, radio) ambiguous blending has been studied under the topic of *confusion limit*, which is approached when the source density of detected objects per beam (or full-width-half-max) approaches $\sim 1/30$ (Scheuer 1957; Condon 1974). Most of these studies are concerned with the associated number and flux count uncertainties (e.g. Oliver et al. 1997), although Hogg (2001) considered astrometric uncertainties related to confusion errors. In this letter, we will for the first time demonstrate that the ellipticity distribution of ambiguously blended objects (as seen from the ground) is different from that of the remaining objects and that this difference has a significant impact on cosmic shear infer-

will@dawsonresearch.com

¹ Lawrence Livermore National Laboratory, P.O. Box 808 L-210, Livermore, CA, 94551, USA.

² University of California, Davis, Physics Department, One Shields Av., Davis, CA 95616, USA

³ <http://lsst.org>

ence.

2. THEORETICAL MODEL

Despite the complex parameter space in which blending occurs, with a simple model, we can understand why a population of ambiguous blends can have an ellipticity distribution qualitatively different from that of non-blended galaxies. As well as determine the effect these ambiguous blends have on shear noise.

2.1. Ellipticity Distribution of Ambiguous Blends

For a population of galaxies randomly distributed on the sky (i.e. ignoring clustering) with surface number density n , the probability of galaxy i having a partner galaxy j a distance r_{ij} away is,

$$p(\text{pair}) \propto 2\pi n r_{ij} dr_{ij}. \quad (1)$$

That is, the probability of a blended pair of galaxies increases linearly with the projected pair separation, r_{ij} .

As the separation increases the two galaxies will become separately resolved, so the ambiguous blend probability must decrease with increasing r_{ij} . To estimate the ambiguous blend probability assume that the galaxies have Gaussian surface brightness profiles with sizes (σ_1, σ_2) , centroids (μ_1, μ_2) , and separation $r_{ij} = |\mu_2 - \mu_1|$ as illustrated in Figure 1. We then define the depth (d) of the trough between the galaxy intensity peaks relative to some noise level (σ_{rms}) as,

$$\Delta \equiv \frac{d}{\sigma_{\text{rms}}}.$$

Then the probability of being able to detect two galaxies as blended is,

$$p(\text{detect blend}) = \int dr_{12} \Delta(r_{12}, A_1, \sigma_1, A_2, \sigma_2) p(A_1) p(\sigma_1) p(A_2) p(\sigma_2) dA_1 d\sigma_1 dA_2 d\sigma_2, \quad (2)$$

where A_i represents the flux of galaxy i and $p(A)$, $p(\sigma)$ are the prior distributions for the intrinsic fluxes and sizes of the galaxies in a catalog after convolution with a PSF. Conceptually this reduces to the fact that as the signal-to-noise ratio (SNR) of the trough (Δ) becomes large, the probability of being able to detect the two galaxies as blended increases. Then the probability density function of ambiguous blends under the assumption of randomly distributed galaxies is the joint probability distribution,

$$p(\text{cat blend}) = \int p(\text{pair}) (1 - p(\text{detect blend})) dr_{12} dA_1 d\sigma_1 dA_2 d\sigma_2. \quad (3)$$

We now consider the case of a population of galaxies with equal amplitudes and sizes, i.e. $p(A_1) = p(A_2) = \delta_D(A)$ and $p(\sigma_1) = p(\sigma_2) = \delta_D(\sigma)$, with $\delta_D(\cdot)$ the Dirac delta function. For analytic simplicity we assume that σ_{rms} is drawn from a one-sided Gaussian. Then the probability of failing to detect a blend reduces to,

$$1 - p(\text{detect blend}) = 1 - \frac{\text{erf}(\Delta/\sqrt{2})}{2}, \quad (4)$$

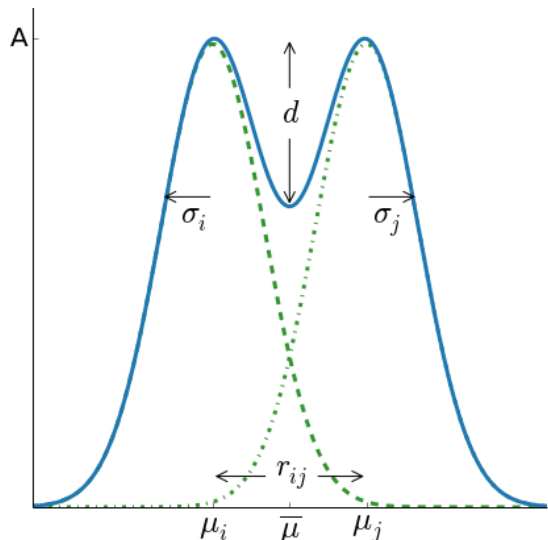


Figure 1. Diagram of two blended galaxies with Gaussian projected surface brightness profiles (green dash and dot-dash curves), located at μ_i and μ_j with sizes σ_i and σ_j . The combined surface brightness profile (blue curve) has a trough depth d .

which is shown by the blue line in Figure 2. For a uniform galaxy population,

$$d \approx A_{12}(\mu) - A_{12}(\bar{\mu}),$$

where $A_{12}(\mu)$ is the sum of the two Gaussian profiles at μ_1 or μ_2 , and $A_{12}(\bar{\mu})$ is the sum of the two Gaussian profiles at the midway point. The resulting probability for ambiguous blends from Equation 3 $p(\text{cat blend} | r_{12}, \sigma)$ is shown as the black curve in Figure 2.

Under our assumption of circular Gaussian galaxies, we can transform pair separation into the ellipticity of the blended pair. The standard ellipticity estimator is defined in terms of the pixel intensity second moments Q_{ij} ,

$$|e|^2 \equiv \frac{(Q_{11} - Q_{22})^2 + Q_{12}^2}{(Q_{11} + Q_{22})^2}.$$

One can show that $|e|$ is a quadratic function of the pair separation when the separation is comparable to or smaller than the galaxy sizes (as is the case for ambiguous blends),

$$|e| = \frac{Mr_{12}^2 + (C_{11} - C_{22})}{Mr_{12}^2 + (C_{11} + C_{22})}, \quad (5)$$

where C is a linear combination of the 2D covariances Σ of each galaxy intensity profile and M is a constant depending on the relative galaxy fluxes. When $r_{12} \ll \sigma \sim \sqrt{C_{ii}}$, $|e| \sim r_{12}^2 / (C_{11} + C_{22})$. So, Figure 2 will look similar when expressed as ellipticity magnitude, except with a quadratic rather than linear relation for small ellipticity. Marginalizing over the full population of galaxy properties will smooth out this offset peak in the ellipticity distribution, however the general trend of larger ellipticity distribution of the ambiguous blended population compared to the non-blended population will remain.

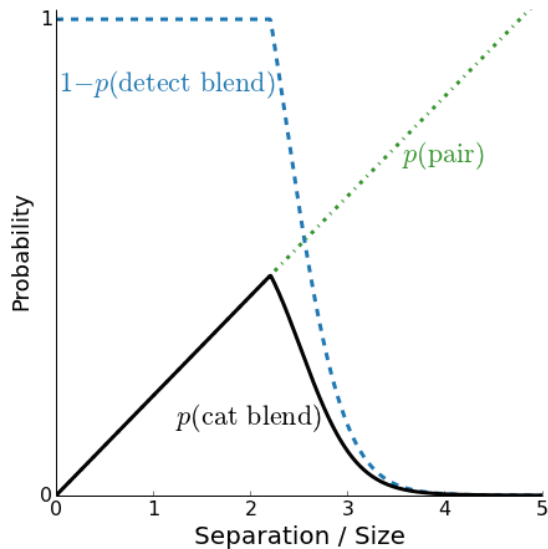


Figure 2. Diagram of the probability distributions involved in determining the ellipticity distribution of ambiguous blends as a function of the galaxy pair separation normalized by their size (assuming two equal size, round, SNR=20 galaxies). The probability of there being a pair of galaxies with a given separation (linear green dot-dash curve) joined with the probability of being unable to detect the pair as blended (blue dash curve), results in probability density function for ambiguous blends with galaxies of those properties throughout the survey.

2.2. Effect of Ambiguous Blends on Shear Noise

We now demonstrate why ambiguous blends increase shear noise, and derive an expression that will quantify the increase in shear noise for a given survey number density of galaxies. Assuming cosmic shear is estimated as the weighted mean shear $\hat{\gamma}$ of a sample of galaxies then the shear noise can be defined as,

$$\hat{\sigma}_\gamma^2 = \frac{\sigma_{\text{SN}}^2}{n_{\text{eff}}},$$

where σ_{SN}^2 is the intrinsic galaxy shape noise, and n_{eff} is the effective number density of galaxies used in the shear measurement (see e.g. Chang et al. 2013). Assuming shape measurement noise is approximately the same for blended and non-blended galaxies we can disregard it without affecting the conclusions. Furthermore we ideally assume that blended objects contain pure lensing signal. This disregards potential noise and bias resulting from the blended objects at disparate redshifts being sheared by different amounts. While important, such complexities are beyond the scope of this letter. Under these assumptions,

$$\hat{\sigma}_\gamma^2 = \frac{\sigma_{\text{SN}}^2}{n_{\text{obs}}} = \frac{n_{\text{B}}\sigma_{\text{SN,B}}^2 + n_{\text{NB}}\sigma_{\text{SN,NB}}^2}{(n_{\text{B}} + n_{\text{NB}})^2},$$

where we now account for the ambiguous blend population (B) and the remaining ‘non-blend’ population (NB) properties, the sum of which account for number density of observed galaxies n_{obs} .

Ambiguous blending will cause an increase in the shear noise by: 1) increasing σ_{SN}^2 , due to $\sigma_{\text{SN,B}}^2$ being greater than $\sigma_{\text{SN,NB}}^2$, and 2) decreasing n_{obs} since multiple objects make up a single blend. To quantify the effects of these contributions we first define β to be the aver-

age number of composite objects per ambiguous blend. Thus $n_{\text{NB}} \equiv n - \beta n_{\text{B}}$, where again n is the raw unblended number density of objects for a given limiting magnitude. The number density of ambiguous blends n_{B} will be proportional to some power of the total pure number density of observable objects, $n_{\text{B}} \equiv \nu n^\alpha$. In the limit that n times the average object area $\gg 1$, then the confusion limit has been reached and both ν and $\alpha \rightarrow 1$. In the limit that n times the average object area $\ll 1$ (as will be the case for most upcoming ground based optical surveys),

$$n_{\text{B}} \propto \sum_i^n p_i(\text{pair}),$$

where $p(\text{pair}) \propto n$, and $\alpha \geq 2$. α will be greater than 2 in part due to clustering, but to a larger degree indirectly from the $p(\text{detect blend})$ term’s dependence on Δ , see Equations 3 & 4. Since $n \sim 10^{0.31(m-20)}$ (Beckwith et al. 2006; Tyson 1988), where m is the limiting apparent z_{850} magnitude of the survey, the number of low signal-to-noise galaxies increases as the limiting magnitude increases. The separation/size phase space where $p(\text{detect blend})=0$ will be larger for these low signal-to-noise galaxies and thus they will have a larger probability of contributing to an ambiguous blend in addition to the n proportionality from $p(\text{pair})$, see Equation 3. Thus α is expected to increase as a survey’s limiting magnitude increases. In light of ambiguous blending the shear variance takes the following form,

$$\hat{\sigma}_\gamma^2 = \frac{[(1 - \beta\nu n^{\alpha-1})\sigma_{\text{SN,NB}}^2 + \nu n^{\alpha-1}\sigma_{\text{SN,B}}^2]}{n[1 - \nu n^{\alpha-1}(\beta - 1)]^2} \quad (6)$$

3. METHOD

We utilize fields with overlapping Subaru:SuprimeCam and HST:ACS coverage to test our theoretical expectation that ambiguously blended objects will have an ellipticity distribution with preferentially larger ellipticities than the ellipticity distribution of non-blended galaxies, and quantify the effect of these blends on the shear noise. Since the HST PSF is approximately an order of magnitude smaller than the Subaru PSF it enables us to identify ambiguous blends in the Subaru catalog.

3.1. Data

We use existing lensing quality Subaru and HST image data for the Musket Ball Cluster field (Dawson et al. 2012). The Subaru data has $0.72''$ seeing, which is close to the expected mean seeing of future ground based lensing survey telescopes (e.g. $0.7''$ for LSST; LSST Science Collaboration et al. 2009). After applying quality cuts based on shape error ($0 < \delta e < 0.3$) and magnitude error (< 0.2), there remain 2356 objects, or ~ 100 objects per arcmin², within the approximate HST field of view. The limiting i -band magnitude is ~ 27 . The HST catalog contains 4637 objects, or ~ 200 objects per arcmin², after applying quality cuts based on shape ($|e| < 0.9$), shape error ($0 < \delta e < 0.3$), size (flux radius > 1.2 pixels), and magnitude error (< 0.2). The limiting F814W magnitude is ~ 28 , and we exclude any objects fainter than 27. Compared with both of the GOODS fields (Giavalisco et al. 2004) we estimate that the fraction of ambiguous blends

in the Musket Ball Cluster data is ~ 1.3 times greater than the field.

3.2. Blend Identification

Our objective for this work is to divide the Subaru objects into blend (i.e. ambiguous blend) and non-blend (i.e. remaining) samples. For each Subaru object we match the closest HST object within a $2''$ radius. These HST objects are defined as *primary matches*. For each HST object not classed as a primary match, we identify the corresponding Subaru object with the least effective separation,

$$r_{\text{eff},ij} = \frac{r_{ij}}{\Xi_{\sigma}(\sigma_i + \sigma_j)},$$

where r_{ij} is the separation of the of HST object i and Subaru object j , σ_i is the size (following the convention of §2) of the HST object after convolution with a Gaussian kernel representative of the Subaru image seeing, σ_j is the size of the Subaru object as measured in the Subaru image, and Ξ_{σ} is a normalizing scale factor. When $r_{\text{eff},ij} < 1$ the two objects are separated by less than Xi_{σ} times the total size of the objects, and the Subaru object j is flagged as a potential blend. Based on visual inspection we find that $\Xi_{\sigma} = 1$ sets a reasonable criteria for identifying nearly all ambiguous blends, with minor non-blend contamination (see §4 for details). Finally we visually inspect all Subaru objects flagged as potential blends to increase the purity of our blended sample.

4. RESULTS

The automated detection scheme identifies 18% of the total number of Subaru objects as being part of ambiguous blends. After visual inspection of these objects in the HST imaging, we confirm that 79% (341) are actually ambiguous blends, or 14% of the total Subaru objects. Most of the false blend detections come from the periphery of the HST field, where there are fewer exposures in the HST images due to dithering, resulting in artifacts such as cosmic rays and noise fluctuations being detected as galaxies. The next largest class of false blend detections come from objects being improperly segmented during the HST reduction, such as face on spiral galaxies with pockets of bright star formation.

From our discussion in §2 we expect that the ambiguous blend population should have larger shape noise than the unblended population (which we now loosely define as non-ambiguous blends). It is shown in Figure 3 that this is the case. The root mean square (RMS) ellipticity of the blended and non-blended distributions are 0.34 and 0.30, respectively. To examine the statistical significance that the two ellipticity distributions are significantly different we create a Q-Q plot, Figure 4, and estimate the variance based on 1000 bootstrap realizations of each population.

By examining these ambiguous blends relative to the HST catalog we are able to estimate the α , β , and ν parameters discussed in §2. We find that $\beta=2.4$, meaning each Subaru ambiguous blend is on average composed of 2.4 HST detected objects. This is a heavy tailed distribution though and $\sim 75\%$ of the blends are composed of just two objects. By ordering the HST objects from brightest to faintest we are able to explore how various ambiguous blend and non-blend quantities vary as a function

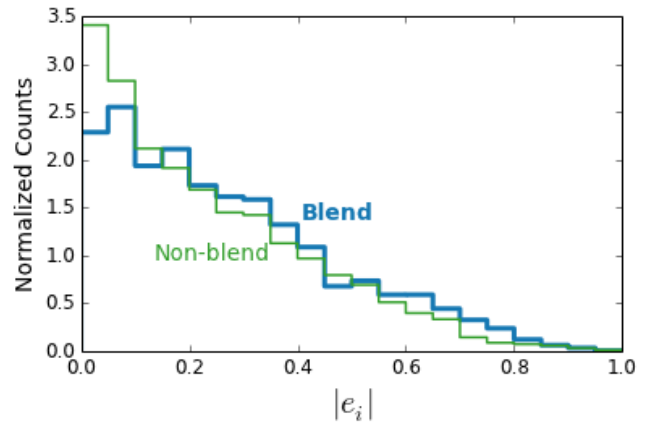


Figure 3. Histograms of the galaxy ellipticity component magnitude as measured from the ground (Subaru). The ambiguous blend ellipticity distribution (thick blue line) is slightly more variable, with $\sigma_{\text{SN,B}} = 0.34$, than the ellipticity distribution of the remainder of the objects (thin green line) with $\sigma_{\text{SN,NB}} = 0.30$.

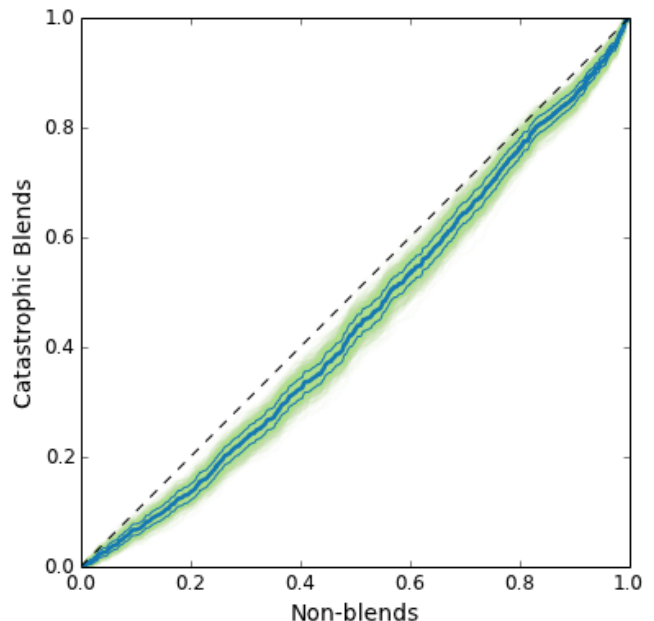


Figure 4. A Q-Q plot (thick blue curve) of the galaxy ellipticity component magnitude $|e_i|$, as measured from the ground (Subaru), for the ambiguous blend population vs. the remaining population. The thin blue curves show the 68% deviations based on 1000 bootstrap realizations of the two populations (overlapping green curves). The composite green curves very nearly represent the 3σ confidence region. Deviation from the 1:1 dashed line shows that the ambiguous blend population has a significantly different ellipticity distribution than the remaining galaxies.

of a survey's limiting raw number density n , see Figure 5. This is done by progressively stepping through the ordered HST catalog and considering correspondingly matched Subaru objects, in this manner a Subaru object transitions from non-blend to blend once two matched HST objects are encountered. Fitting a power law to the n_B curve of Figure 5 we find that $\nu=(2.3\pm 0.07)\times 10^{-6}$ and $\alpha=3.15\pm 0.007$, with $\Sigma_{\nu\alpha}=-4.9\times 10^{-10}$. Referring to Equation 6, and given the α , β , and ν parameter estimates as well as the RMS ellipticity of the blended and non-blended populations we find that blending results in a shear noise increase of $\sim 14\%$. This is essentially equiv-

alent to a 12% decrease in the effective number density of galaxies n_{eff} . Recall from §2.2 that this optimistically assumes pure lensing signal from the ambiguous blends.

We now consider the sample of Subaru galaxies which would qualify as the LSST Gold Sample ($i < 25.3$), since these are what will eventually be used for the primary cosmic shear measurements (LSST Science Collaboration et al. 2009; LSST Dark Energy Science Collaboration 2012). While we only use galaxies with $i < 25.3$ to estimate the ambiguous blend and non-blend population properties, we consider all galaxies ($i \lesssim 27$, which is approximately the LSST limiting magnitude) when determining which of the $i < 25.3$ galaxies are ambiguous blends. We still find that the blend and non-blend ellipticity distributions are significantly different in a Q-Q plot, however we find that the RMS ellipticity of the blended populations reduces from 0.34 to 0.32. Below $|e_i| \sim 0.5$ the blend distribution looks nearly identical to that in Figure 3, however above $|e_i| \sim 0.5$ there is almost no difference between the blend and non-blend population. For this subsample we find that ambiguous blending results in a shear noise increase of $\sim 7\%$ versus a sample without ambiguous blends, which is essentially equivalent to a 7% decrease in the effective number density of galaxies. This suggests that upon further investigation the blending related shear noise metric, Equation 6, could be coupled with other lensing quality metrics to determine an optimal LSST Gold Sample.

5. DISCUSSION & CONCLUSIONS

We have shown that the distribution of ellipticities of ambiguously blended galaxies is different from that of unblended galaxies. We can understand the shape of the ellipticity distribution for blended galaxies with a simple geometric interpretation, independent of the morphological characteristics of the galaxies (which give perturbations about the geometric result). The key feature of the blended galaxy ellipticity distribution is a peak that is offset from zero, with the mode of the distribution increasing roughly quadratically with the size of the seeing-limited PSF.

Combined with the ellipticity distribution of unblended galaxies, the intrinsic ellipticity dispersion of all galaxies $\sigma_{e,\text{int}}$ increases as the blended fraction increases. This increases the shape noise for weak lensing measurements over what would be measured with a much smaller PSF (e.g. from space). Because the fraction of blended objects increases with increasing source galaxy number density, the shape noise also therefore decreases more slowly than $\sqrt{N_{\text{gal}}}$ in the presence of significant blending. Both of these effects make the characterization of the blended ellipticity distribution paramount for accurate shape noise modeling and mitigation for weak lensing in future deep surveys.

In the context of probabilistic weak lensing analysis (Miller et al. 2007; Bernstein & Armstrong 2014), neglecting the modifications to the intrinsic ellipticity distribution from blending can lead to overconfident and biased cosmological parameter inference through marginalization over a prior that is too narrow.

ACKNOWLEDGMENTS

We thank the LSST DESC members for many valuable conversations related to this work, in particular David

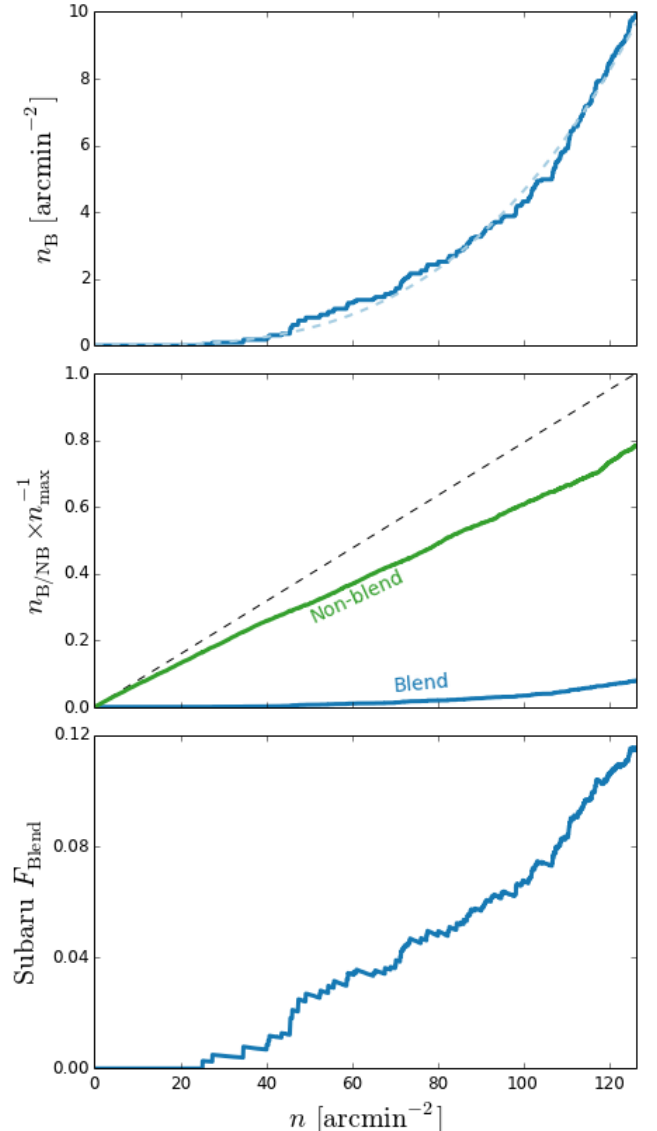


Figure 5. *Top panel:* the cumulative number of ambiguously blended objects per arcmin^2 (n_B) in the ground based Subaru observations as a function of the corresponding number density of underlying objects observed by HST (n), ordered from brightest to faintest. (Recall from §1 n is different than the number density of a subsample or that observed from the ground.) The faint end slope (corresponding to larger n) is steeper due to these galaxies being lower signal to noise and thus more likely to contribute to an ambiguous blend, see discussion in §2. The light dashed blue line shows the best fit power law $2.3e-6 \times n^{3.15}$. *Middle panel:* The number density of ambiguous blends (blue curve) and remaining objects (green curve) relative to the total number density of HST objects. The Blend and Non-blend curves do not sum to give the dashed black curve since at least two objects are required to make a single ambiguous blend. *Bottom panel:* Fraction of Subaru detected objects that are verified ambiguous blends. Compare with Figure 8 of Chang et al. (2013).

Kirkby and Andrew Bradshaw. Part of this work performed under the auspices of the U.S. DOE by LLNL under Contract DE-AC52-07NA27344. This material is based upon work supported by the NSF under Grant No. AST-1108893. Support for program number GO-12377 was provided by NASA through a grant from STScI, which is operated by AURA, under NASA contract NAS5-26555. Based in part on data collected at

Subaru Telescope, which is operated by NOAJ.

REFERENCES

- Beard, S. M., MacGillivray, H. T., & Thanisch, P. F. 1990, MNRAS, 247, 311
- Beckwith, S. V. W., Stiavelli, M., Koekemoer, A. M., et al. 2006, AJ, 132, 1729
- Bernstein, G. M. 2010, MNRAS, 406, 2793
- Bernstein, G. M., & Armstrong, R. 2014, MNRAS, 438, 1880
- Bertin, E., & Arnouts, S. 1996, A&AS, 117, 393
- Chang, C., Jarvis, M., Jain, B., et al. 2013, MNRAS, 434, 2121
- Condon, J. J. 1974, ApJ, 188, 279
- Dawson, W. A., Wittman, D., Jee, M. J., et al. 2012, ApJ, 747, L42
- Giavalisco, M., Ferguson, H. C., Koekemoer, A. M., et al. 2004, ApJ, 600, L93
- Hogg, D. W. 2001, AJ, 121, 1207
- Kacprzak, T., Zuntz, J., Rowe, B., et al. 2012, MNRAS, 427, 2711
- Miller, L., Kitching, T. D., Heymans, C., Heavens, A. F., & van Waerbeke, L. 2007, MNRAS, 382, 315
- Miller, L., Heymans, C., Kitching, T. D., et al. 2013, MNRAS, 429, 2858
- Oliver, S. J., Goldschmidt, P., Franceschini, A., et al. 1997, MNRAS, 289, 471
- Scheuer, P. A. G. 1957, Proceedings of the Cambridge Philosophical Society, 53, 764
- Tyson, J. A. 1988, AJ, 96, 1
- Voigt, L. M., & Bridle, S. L. 2010, MNRAS, 404, 458
- LSST Science Collaboration, Abell, P. A., Allison, J., et al. 2009, arXiv:0912.0201
- LSST Dark Energy Science Collaboration 2012, arXiv:1211.0310
- Bridle, S., Balan, S. T., Bethge, M., et al. 2010, MNRAS, 405, 2044
- Mandelbaum, R., Rowe, B., Bosch, J., et al. 2014, ApJS, 212, 5